Crystal Structures of SgcE6 and SgcC, the Two-Component Monooxygenase that Catalyzes Hydroxylation of a Carrier Protein-Tethered Substrate in Biosynthesis of the Enediyne Antitumor Antibiotic C-1027 in *Streptomyces globisporus*

Chin-Yuan Chang,[1,†] Jeremy R. Lohman,[1,†] Hongnan Cao,[2] Kemin Tan,[3] Jeffrey D. Rudolf,[1] Ming Ma,[1] Weijun Xu,[2] Craig A. Bingman,[4] Ragothaman M. Yennamalli,[2,5] Lance Bigelow,[3] Gyorgy Babnigg,[3] Xiaohui Yan,[1] Andrzej Joachimiak,[3] George N. Phillips, Jr.,[2] and Ben Shen*,[1,6,7]

[1]Department of Chemistry, The Scripps Research Institute, Jupiter, FL 33458, United States; [2]BioScience at Rice and Department of Chemistry, Rice University, Houston, TX 77251, United States; [3]Midwest Center for Structural Genomics and Structural Biology Center, Biosciences Division, Argonne National Laboratory, Argonne, IL 60439, United States; [4]Department of Biochemistry, University Wisconsin-Madison, Madison, WI 53705, United States; [5]Department of Biotechnology and Bioinfomatics, Jaypee University of Information Technology, Waknaghat, Himachal Pradesh, India 173234, and [6]Department of Molecular Therapeutics and [7]Natural Products Library Initiative at The Scripps Research Institute, The Scripps Research Institute, Jupiter, FL 33458, United States

[†]These authors contributed equally

*Correspondence: E-mail: shenb@scripps.edu. Telephone: (561) 228-2456. Fax: (561) 228-2472.

Supporting Information

Table S1.	Primers and vectors used in this study	S2
Table S2.	Homologues of SgcE6 discussed in this study	S3
Table S3.	Homologues of SgcC discussed in this study	S5
Figure S1.	The top ten templates used by I-TASSER for SgcC2 modeling	S7
Figure S2.	Sequence alignment of SgcE6 with selected homologues	S8
Figure S3.	Sequence alignment of SgcC with selected homologues	S9
Figure S4.	Stereoimage of SgcE6 monomer alignment	S10
Figure S5.	Structural comparison of SgcE6 with other flavin reductases	S11
Figure S6.	Molecular weight estimation of SgcE6 and SgcC	S12
Figure S7.	Reactions carried out by SgcC homologous enzymes	S13
Figure S8.	Structure based sequence alignment identity matrix	S14
Figure S9.	Comparison of SgcC and TtHpaB in stereograms	S15
Figure S10.	Active site of AbHpaH	S16
Figure S11.	The SgcC-SgcC2 docking model	S17
References		S18

Table S1. Primers and vectors used in this study.

Plasmid	PCR primers	Cloning vector
APC109096 (pBS1159)	SgcE6-F: 5'-TACTTCCAATCCAATGCCATGAGTCCGATCATCGCTCCG-3'	pMCSG73
	SgcE6-R: 5'-TTATCCACTTCCAATGTTATGCCGCCCTTCCTTCGTCC-3'	
APC109081 (pBS1160)	SgcC-F: 5'-AAAACCTCTATTTCCAGTCGCCCCACGGTGCAGAGCGCG-3'	pBS3080
	SgcC-R: 5'-TACTTACTTAAATGTTACAGCCCTCCGAGAAGGTCG-3'	

Table S2. Homologues of SgcE6 discussed in this study.

Organism	Abbreviation	Substrate (Fixed concentration)	Second substrate	K_m (μM)	K_{cat} (s^{-1})	DALI analysis					Accession number	PDB ID	Reference
						%id[a]	Z[b]	rmsd[c]	lali[d]	nres[e]			
Streptomyces globisporus	SgcE6	FAD	NADH	8.2	4.5	-	-	-	-	-	AAL06698	4R82, 4HX6	**1**
		FMN	NADH	Very low activity									
		NADH	FAD	53	3.1								
		NADPH	FAD	Below detection									
Thermus thermophilus HB8	TtHpaC	FAD	NADH	8.9	2.4	33	22.5	1.6	147	149	BAD70784	2ED4, 2ECR, 2ECU	**2**
		FMN	NADH	39.6	2.7								
		NADH	FAD	36.8	0.7								
		NADPH	FAD	Below detection									
Bacillus thermoglucosidasius A7	BtPheA2	FAD	NADH	1.5	252	34	24.1	1.4	149	153	AAF66547	1RZ1, 1RZ0	**3, 4**
		FMN	NADH	5.4	279								
		NADH	FAD	8.8	225								
		NADPH	FAD	Very low activity									
Burkholderia cepacia AC1100	BcTftC	FAD	NADH	4.8	16.6	22	22.6	1.9	156	164	AAC23547	3K88, 3K87, 3K86	**5**
		FMN	NADH	10.3	18.5								
		NADH	FAD	40	30.1								
		NADPH	FAD	Not performed									
Pseudomonas putida S12 (*Pseudomonas* sp. VLB120)[f]	PpSMOB	FAD	NADH	11.6	47	28	22.2	1.7	149	152	AJA17114	4F07	**6**
		FMN	NADH	7.1	48								
		NADH	FMN	20.1	60								
		NADPH	FMN	Below detection									
Mycobacterium thermoresistible	MtMOB	No experimental evidence				32	23.2	1.9	60	181	ADR80228	3NFW	**7**

Sulfolobus tokodaii	StHpaC	FMN	NADH	Relative activity: 100%		24	22.1	1.6	152	155	BAB65731	2D37, 2D36, 2D38	**8**
		FMN	NADPH	Relative activity: 5.4%									
		FAD	NADH	Relative activity: 67.5%									
Thermus thermophilus	TtFMNbp	NADPH	FMN	K_d = 17	K_{red} = 0.15	23	21.0	2.0	161	175	BAD71681	2ZOE, 1USC, 1USF	**9**
		NADH	FMN	K_d = 300	K_{red} = 0.25								
		NADPH	FAD	No experimental evidence									
		NADH	FAD										
Pyrococcus horikoshii	PhFMNbp	NADPH	FMN	K_d = 114	K_{red} = 0.06	21	20.4	2.0	156	176	BAA29950	3ZOC, 2R6V	**9**
		NADH	FMN	Below detection									
		NADPH	FAD	No experimental evidence									
		NADH	FAD										
Methanobacterium thermoautotrophicum	MtFMNbp	Structural biology evidence: protein complex with FMN. No experimental evidence for other substrates.				21	19.4	2.2	159	192	AAB84658	1EJE	**10**
Archaeoglobus fulgidus	AfFeR	FMN	NADPH	V_{max} = 280 µmol/min/mg		25	20.4	2.6	150	161	AAB90418	1I0S, 1I0R	**11, 12**
		FAD	NADPH	V_{max} = 350 µmol/min/mg									
		NADPH	FMN	0.3	Not performed								
		NADH	FMN/FAD	Not performed									
Escherichia coli W	EcHpaC	FMN	NADH	2.1	V_{max} = 70 µmol/min/mg	27 (by BLAST)	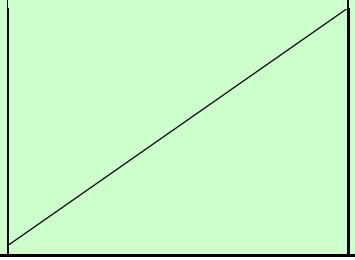				ADT77975	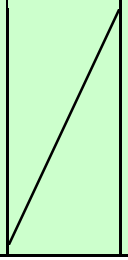	**13**
		FAD	NADH	3.1	V_{max} = 38 µmol/min/mg								
		NADH	FMN	40	Not performed								
		NADPH	FMN	Not performed	V_{max} = 0.5 µmol/min/mg								

[a]%id: percentage of identical amino acids over structurally equivalent residues. [b]Z score: the statistical significance of the similarity between protein-of-interest and other neighbourhood proteins. [c]rmsd: root-mean-square deviation of Cα atoms in the least-squares superimposition of the structurally equivalent Cα atoms. [d]lali: the number of structurally equivalent residues. [e]nres: the total number of amino acids in the hit protein. [f]The kinetics statistics referred to that of the flavin reductase from *Pseudomonas* sp. VLB120. The amino acid sequence identity of PpSMOB and the flavin reductase from *Pseudomonas* sp. VLB120 is 94%.

Table S3. Homologues of SgcC discussed in this study.

Organism	Abbreviation	Flavin	Function	%id[a]	DALI analysis				Accession number	PDB ID	Reference
					Z[b]	rmsd[c]	lali[d]	nres[e]			
Streptomyces globisporus	SgcC	FAD	(S)-3-chloro-β-tyrosyl-*S*-peptidyl carrier protein 5-hydroxylase	-	-	-	-	-	AAL06674	4OO2	**14**
Thermus thermophilus HB8	TtHpaB	FAD	4-hydroxyphenylacetate-3-hydroxylase	34	49.6	1.9	468	470	BAD70783	2YYJ, 2YYG, 2YYI, 2YYK, 2YYL, 2YYM	**15**
Burkholderia cepacia AC1100	BcTftD	FAD	chlorophenol 4-monooxygenase	26	42.7	2.3	461	482	AAC23548	3HWC	**5**
Cupriavidus necator JMP134 (*Ralstonia eutropha*)	CnTcpA	FAD	2,4,6-trichlorophenol 4-monooxygenase	22	22.6	1.9	156	164	AAZ60952	4G5E	**16**
Pseudomonas aeruginosa PAO1	PaHpaA	FAD	4-hydroxyphenylacetate 3-monooxygenase	51					AAG07478		**17, 18**
Escherichia coli	EcHpaB	FAD	4-hydroxyphenylacetic hydroxylase	50					ADT77976		**19, 20, 21**
Bacillus thermoglucosidasius A7 (*Geobacillus thermoglucosidasius*)	BtPheA1	FAD	phenol 2-hydroxylase	51					AAF66546		**22**
Pseudomonas aeruginosa PAO1	PaPvcC	No experimental evidence	putative hydroxylase (involved in pyoverdine chromophore biosynthesis)	42					AAG05644		**23, 24**
Geobacillus thermodenitrificans NG80-2	GtHpaH (GNTG_3160)	FAD	putative aromatic compound hydroxylase	33					ABO68505		**25**
Geobacillus sp. PA-9	GpHpaH	No experimental evidence	4-hydroxyphenylacetic acid 3-hydroxylase	30					AAT28189		**26**
Rhodococcus opacus SAO101 (*Bacillus sphaericus* JS905)	RoNpcA	FAD	4-nitrophenol 4-monooxygenase	28					BAD30042		**27**
Arthrobacter sp. JS443	AjNpdA2	FAD	4-nitrophenol monooxygenase	28					ABL75143		**28**
Oscillatoria sp. PCC 6506	AnaB	FAD	prolyl-ACP dehydrogenase	10	21.5	3.2	313	378	CBN59192	4IRN	**29**

Streptomyces hygroscopicus subsp. *ascomyceticus*	FkbI	FAD	acyl-ACP dehydrogenase	16	20.4	2.9	298	353	AAF86388	1R2J	**30**
Acinetobacter baumannii	AbHpaH	FMN	*p*-hydroxyphenylacetate hydroxylase	7	16.2	3.5	301	399	AAS75429	2JBT, 2JBR, 2JBS	**31**
Bacillus circulans	BtrO	FMN	4-(γ-L-glutamylamino)butanoyl-ACP monooxygenase						BAE07076		**32**

[a]%id: amino acid sequence identity. [b]Z score: the statistical significance of the similarity between protein-of-interest and other neighbourhood proteins. [c]rmsd: root-mean-square deviation of Cα atoms in the least-squares superimposition of the structurally equivalent Cα atoms. [d]lali: the number of structurally equivalent residues. [e]nres: the total number of amino acids in the hit protein.

Figure S1. The top ten threading templates used by I-TASSER for SgcC2 modeling. The residues in template, which are identical to the residue in the query sequence, are highlighted in color. Iden1 is the sequence identity (%) of the templates in the threading aligned region with the query sequence. Iden2 is the sequence identity (%) of the whole template chains with query sequence. Cov represents the coverage of the threading alignment and is equal to the number of aligned residues divided by the length of query protein. Norm. Z-score is the normalized Z-score of the threading alignments.

PDB Hit	Iden1	Iden2	Cov	Norm. Z-score	20 | 40 | 60
					SLEEKVTRIWTGVLGTSGEEGATFIELGGQSVSAVRIATRIQEELDIWVDIGVLFDDPDLPTFIAAVVRT
2mr7:A	0.29	0.37	1.00	2.41	ATEKVLCALYAEILGVEVGVDDAFHDLGGSSALAMRLIARIREELGVDLPIRQLFSSPTPAGVARALAAK
4pwv:A	0.28	0.29	0.97	1.99	ETESRLRRIFEEVLHSEDDVEANFFELGGHSLQATKLVSRIRSEFDAELPLRDFFEHPNVAGLAVLIG--
2jgp:A	0.24	0.27	1.00	3.53	VWEARLAQVWEQVLNVPQGALDDFFALGGHSLRAMRVLSSMHNEYQVDIPLRILFEKPTIQELAAFIEET
2jgp:A	0.24	0.27	1.00	1.80	VWEARLAQVWEQVLNPQVGALDDFFALGGHSLRAMRVLSSMHNEYQVDIPLRILFEKPTIQELAAFIEET
2jgp:A	0.24	0.27	1.00	1.59	VWEARLAQVWEQVLNVPVGALDDFFALGGHSLRAMRVLSSMHNEYQVDIPLRILFEKPTIQELAAFIEET
4pwv:B	0.28	0.29	0.99	3.43	ETESRLRRIFEEVLHSEVDVEANFFELGGHSLQATKLVSRIRSEFDAELPLRDFFEHPNVAGLAVLIGG-
2jgp:A	0.23	0.27	0.99	2.22	VWEARLAQVWEQVLNVPVGALDDFFALGGHSLRAMRVLSSMHNEYQVDIPLRILFEKPTIQELAAFIEE-
2jgp:A	0.24	0.27	1.00	1.10	VWEARLAQVWEQVLNVPVGALDDFFALGGHSLRAMRVLSSMHNEYQVDIPLRILFEKPTIQELAAFIEET
4pwv:B	0.28	0.29	0.99	3.93	ETESRLRRIFEEVLHSEVDVEANFFELGGHSLQATKLVSRIRSEFDAELPLRDFFEHPNVAGLAVLIGG-
4pwv:B	0.28	0.29	0.99	5.04	ETESRLRRIFEEVLHSEVDVEANFFELGGHSLQATKLVSRIRSEFDAELPLRDFFEHPNVAGLAVLIGG-

Figure S2. Sequence alignment of SgcE6 with other 9-membered enediyne gene cluster homologues. Accession numbers are shown in front of their sequences. Aligned residues are colored on the basis of the level of conservation (red box with white character or red character with bold font shows strict identity, red character similarity, and blue frame similarity across group). The sequence in red and magenta correlates with either NADH or NADPH preference, the regions in orange and yellow correlate with FMN or FAD preference and the regions in green and cyan highlight the (S/T/C)XXPP and GDH motifs, respectively. The yellow region corresponds to the "flexible AMP binding loop".

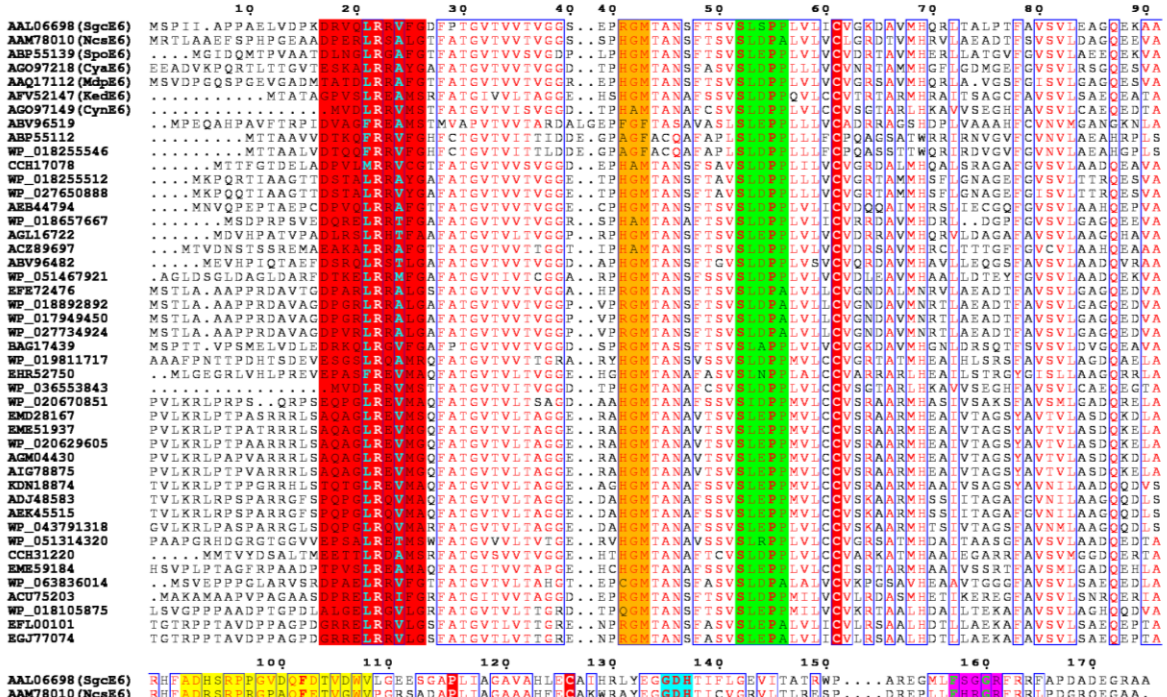

Figure S3. Sequence alignment of SgcC with other 9-membered enediyne gene cluster homologues. Accession numbers are shown in front of their sequences. Aligned residues are colored on the basis of the level of conservation (red box with white character or red character with bold font shows strict identity, red character similarity, and blue frame similarity across group). The regions in yellow, green and magenta are putative flavin binding loop, substrate binding loop and AMP responsive loop, respectively.

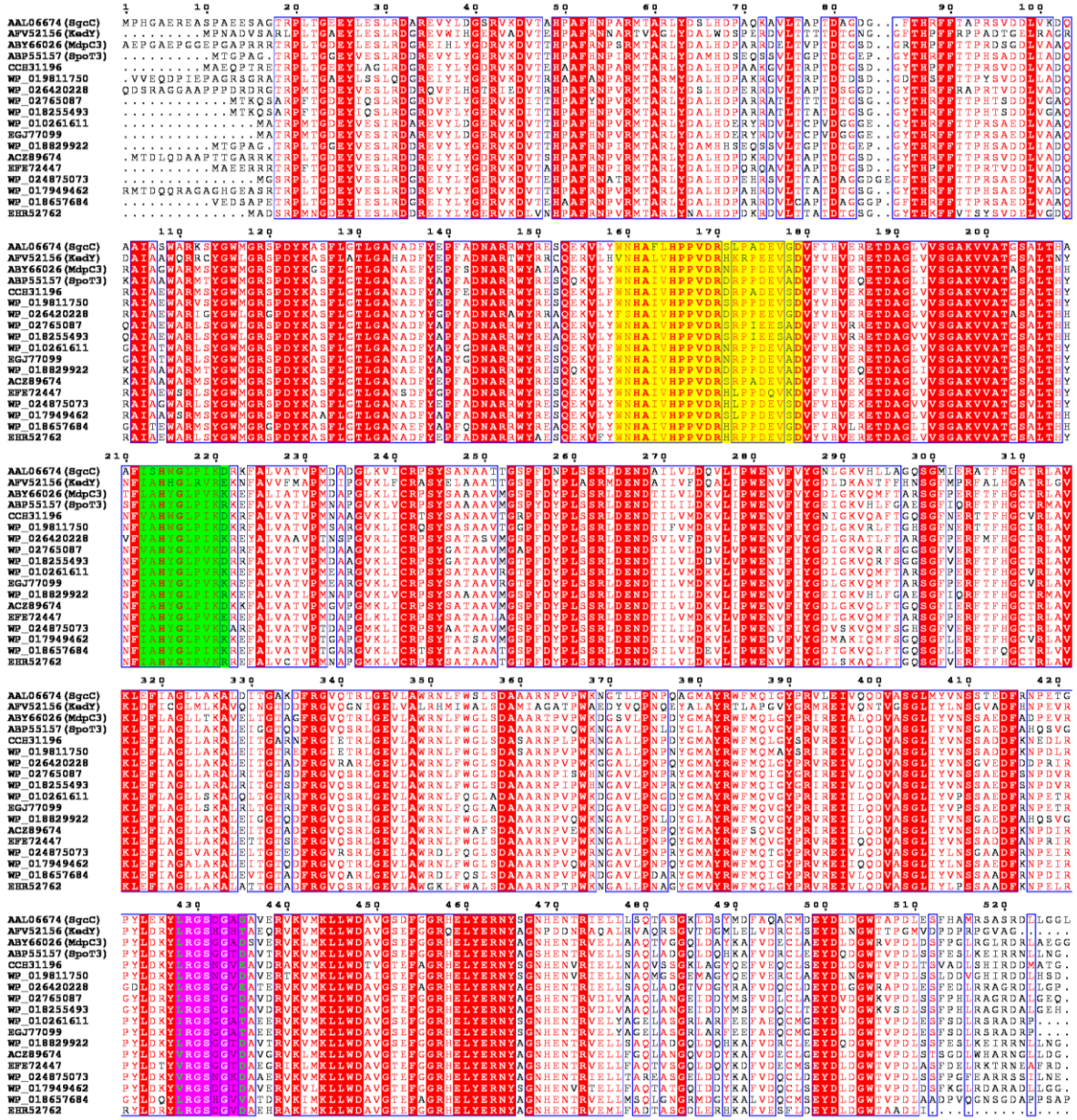

Figure S4. Stereoimage of SgcE6 monomer alignment. The N-terminus, C-terminus and flexible loop are highly variable in position. SgcE6-FAD chain A-black, Apo-SgcE, chain A-green, B-cyan, C-magenta, D-yellow, E-salmon, F-white, G-slate, H-orange.

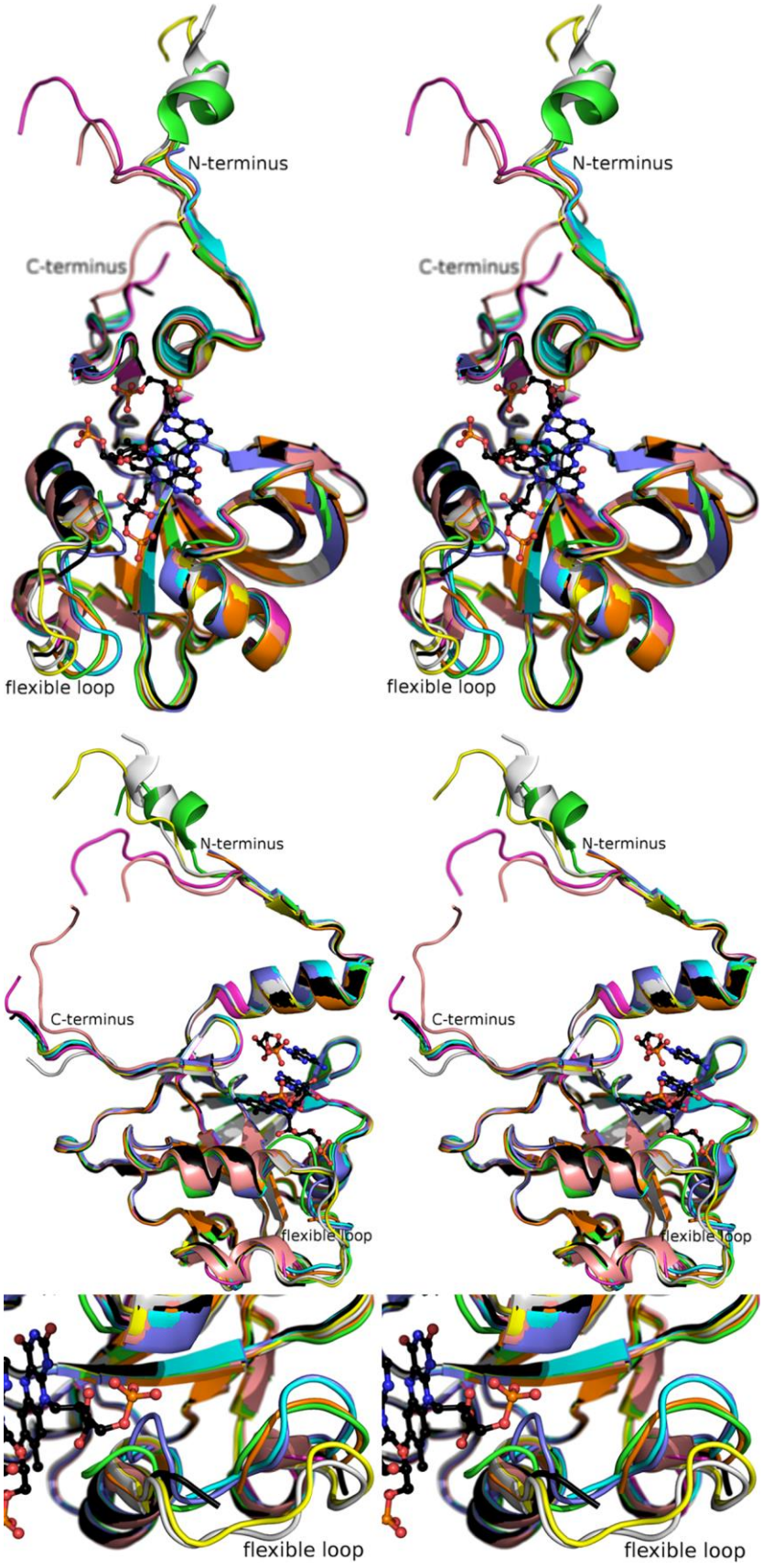

Figure S5. Structural comparison of SgcE6 with other flavin reductases. Colored as seen in Figure 2. The C-terminal loop of MtMOB, which is colored in black, extends into the active site.

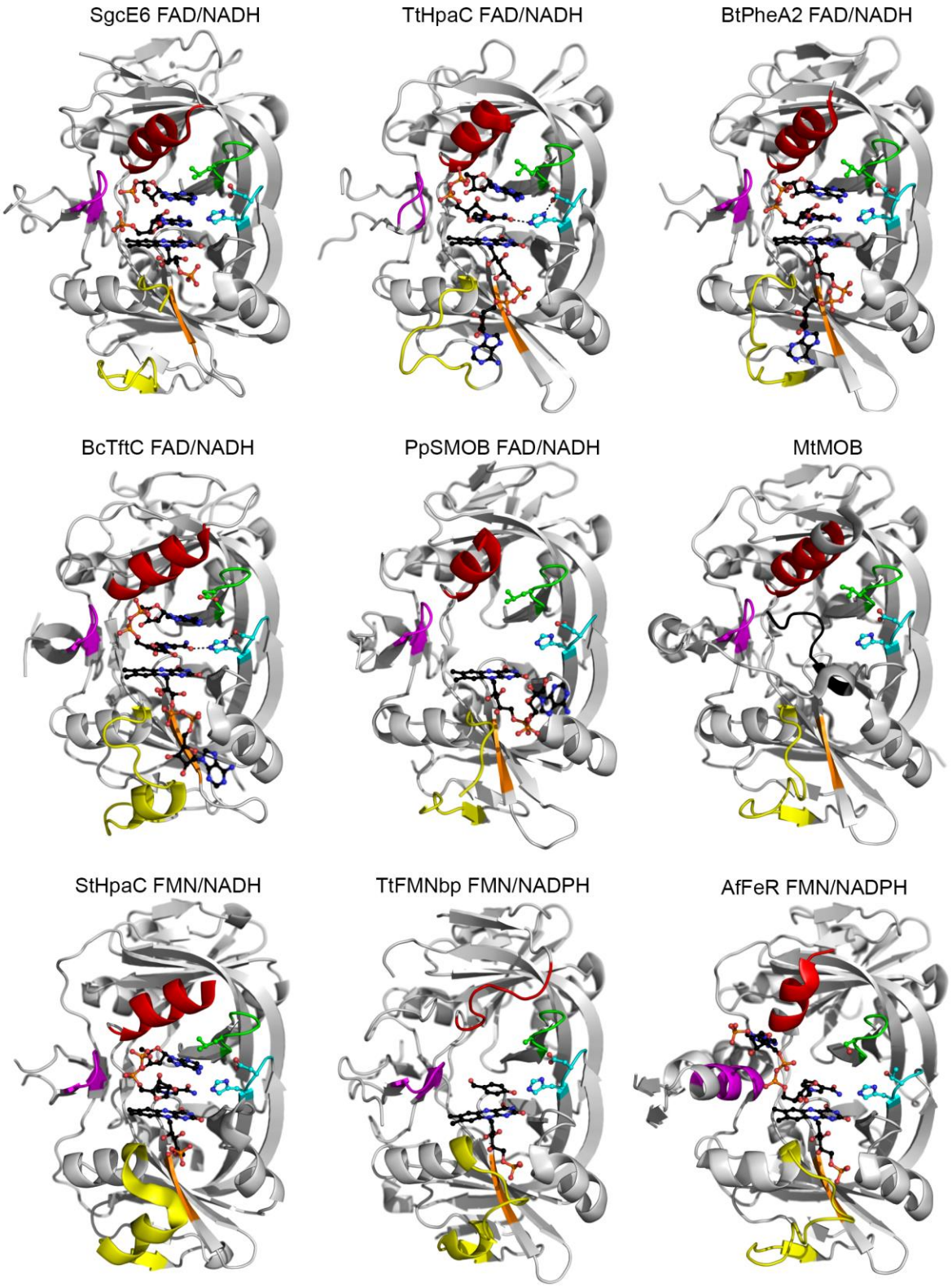

Figure S6. Molecular weight estimation of SgcE6 and SgcC by size exclusion chromatography. (a) SgcE6 and (b) SgcC on a Superdex 200 16/600 column (GE Healthcare Life Science). The apparent molecule weights of SgcE6 and SgcC were estimated to be 46.1 kDa and 209.7 kDa, suggesting that SgcE6 (calculated molecular weight of 19.5 KDa) and SgcC (calculated molecular weight of 57.9 KDa) are dimer and tetramer, respectively.

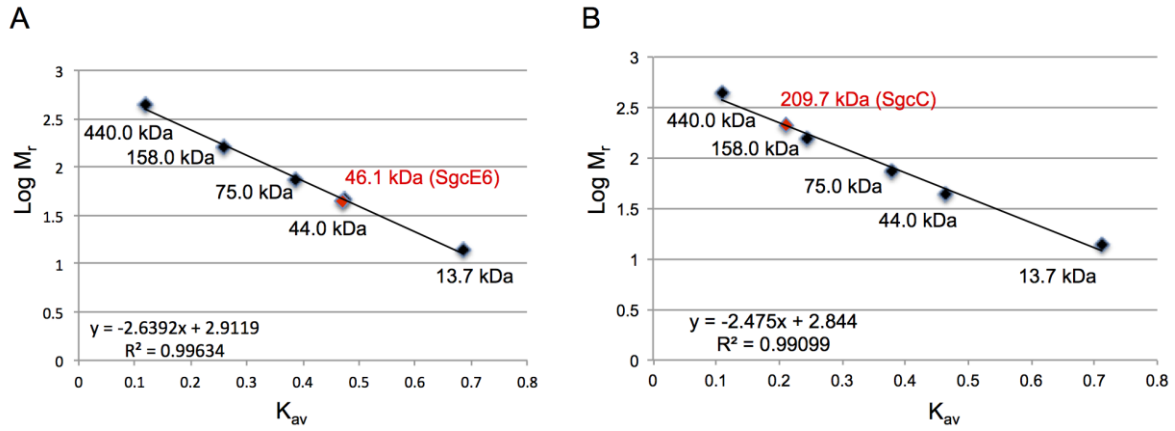

Figure S7. Reactions carried out by SgcC homologous enzymes.

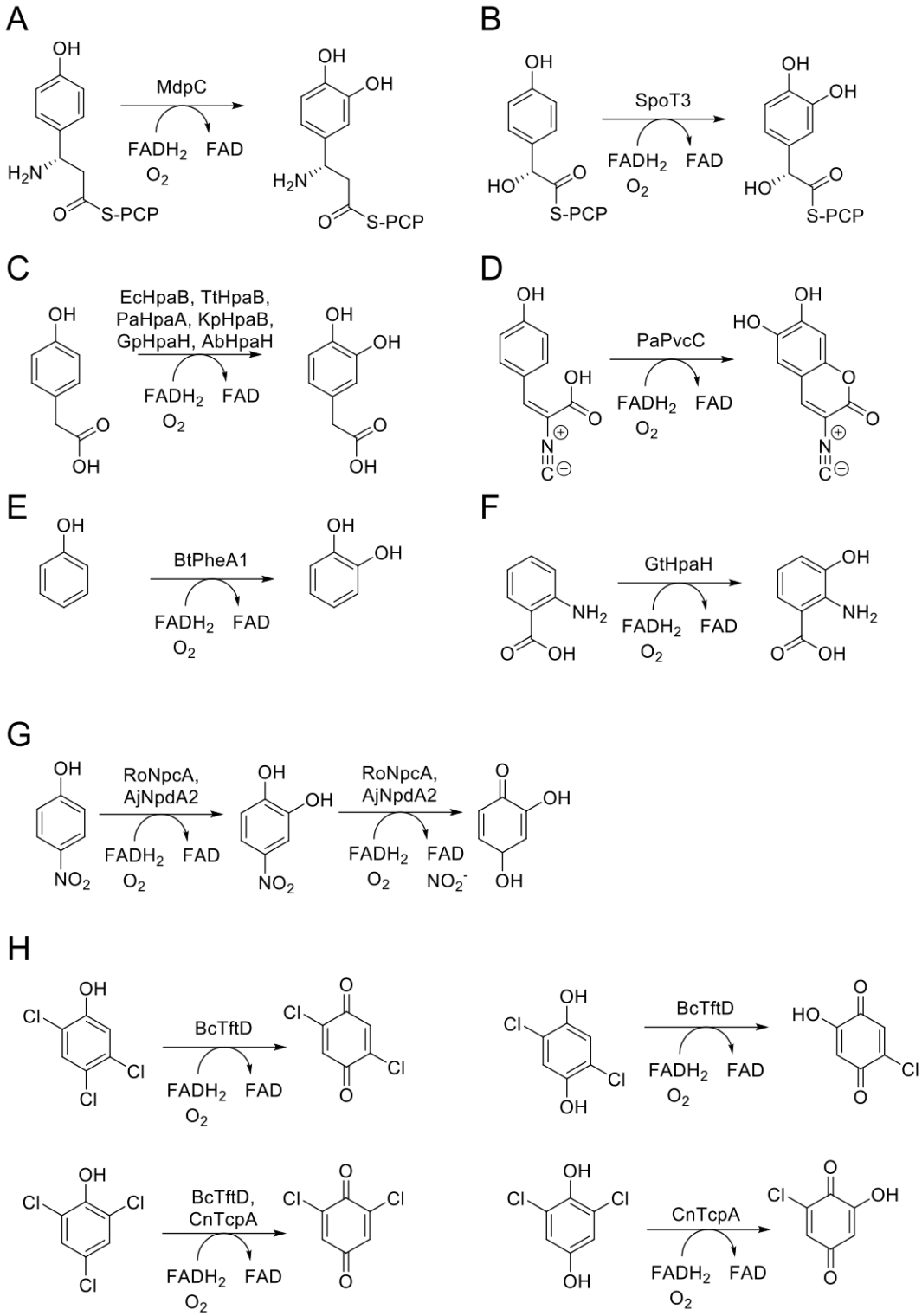

Figure S8. Structure based sequence alignment identity matrix. The sequences for some sequences were left out of Figure 3.

	SgcC	SpoT3	MdpC3	KedY	EcHpaB	PaHpaA	PaPvcC	BtPheA1	TtHpaB	GtHpaH	GpHpaH	BcTftD	CnTcpA	RoNpcA	AjNpdA2
SgcC	1.00	0.72	0.72	0.55	0.49	0.50	0.40	0.48	0.29	0.29	0.26	0.21	0.20	0.22	0.21
SpoT3	0.72	1.00	0.75	0.57	0.51	0.51	0.42	0.50	0.30	0.29	0.27	0.21	0.20	0.22	0.22
MdpC3	0.72	0.75	1.00	0.58	0.50	0.51	0.43	0.50	0.29	0.29	0.25	0.21	0.20	0.21	0.21
KedY	0.55	0.57	0.58	1.00	0.52	0.53	0.45	0.49	0.30	0.30	0.27	0.22	0.21	0.23	0.22
EcHpaB	0.49	0.51	0.50	0.52	1.00	0.72	0.41	0.48	0.26	0.27	0.26	0.22	0.20	0.21	0.21
PaHpaA	0.50	0.51	0.51	0.53	0.72	1.00	0.42	0.50	0.27	0.27	0.27	0.21	0.20	0.23	0.20
PaPvcC	0.40	0.42	0.43	0.45	0.41	0.42	1.00	0.44	0.27	0.31	0.25	0.20	0.20	0.22	0.21
BtPheA1	0.48	0.50	0.50	0.49	0.48	0.50	0.44	1.00	0.29	0.29	0.29	0.23	0.22	0.24	0.22
TtHpaB	0.29	0.30	0.29	0.30	0.26	0.27	0.27	0.29	1.00	0.41	0.47	0.23	0.24	0.25	0.23
GtHpaH	0.29	0.29	0.29	0.30	0.27	0.27	0.31	0.29	0.41	1.00	0.35	0.22	0.22	0.22	0.20
GpHpaH	0.26	0.27	0.25	0.27	0.26	0.27	0.25	0.29	0.47	0.35	1.00	0.21	0.20	0.20	0.19
BcTftD	0.21	0.21	0.21	0.22	0.22	0.21	0.20	0.23	0.23	0.22	0.21	1.00	0.65	0.43	0.41
CnTcpA	0.20	0.20	0.20	0.21	0.20	0.20	0.20	0.22	0.24	0.22	0.20	0.65	1.00	0.43	0.43
RoNpcA	0.22	0.22	0.21	0.23	0.21	0.23	0.22	0.24	0.25	0.22	0.20	0.43	0.43	1.00	0.71
AjNpdA2	0.21	0.22	0.21	0.22	0.21	0.20	0.21	0.22	0.23	0.20	0.19	0.41	0.43	0.71	1.00

Figure S9. Comparison of SgcC and TtHpaB in stereograms. Colors correspond to sequence alignment in Figure 3. (A) Apo TtHpaB is in white and bright colors, SgcC is in gray and dark colors. (B) Apo TtHpaB is similar to panel A, FAD bound TtHpaB is in gray and dark colors. (C) FAD/4-HPA bound TtHpaB is in white and bright colors and FAD bound TtHpaB is similar to panel B. The conformation of the active site loops of TtHpaB changes upon FAD and 4-HPA binding. The conformations seen in SgcC are similar to those of apo TtHpaB.

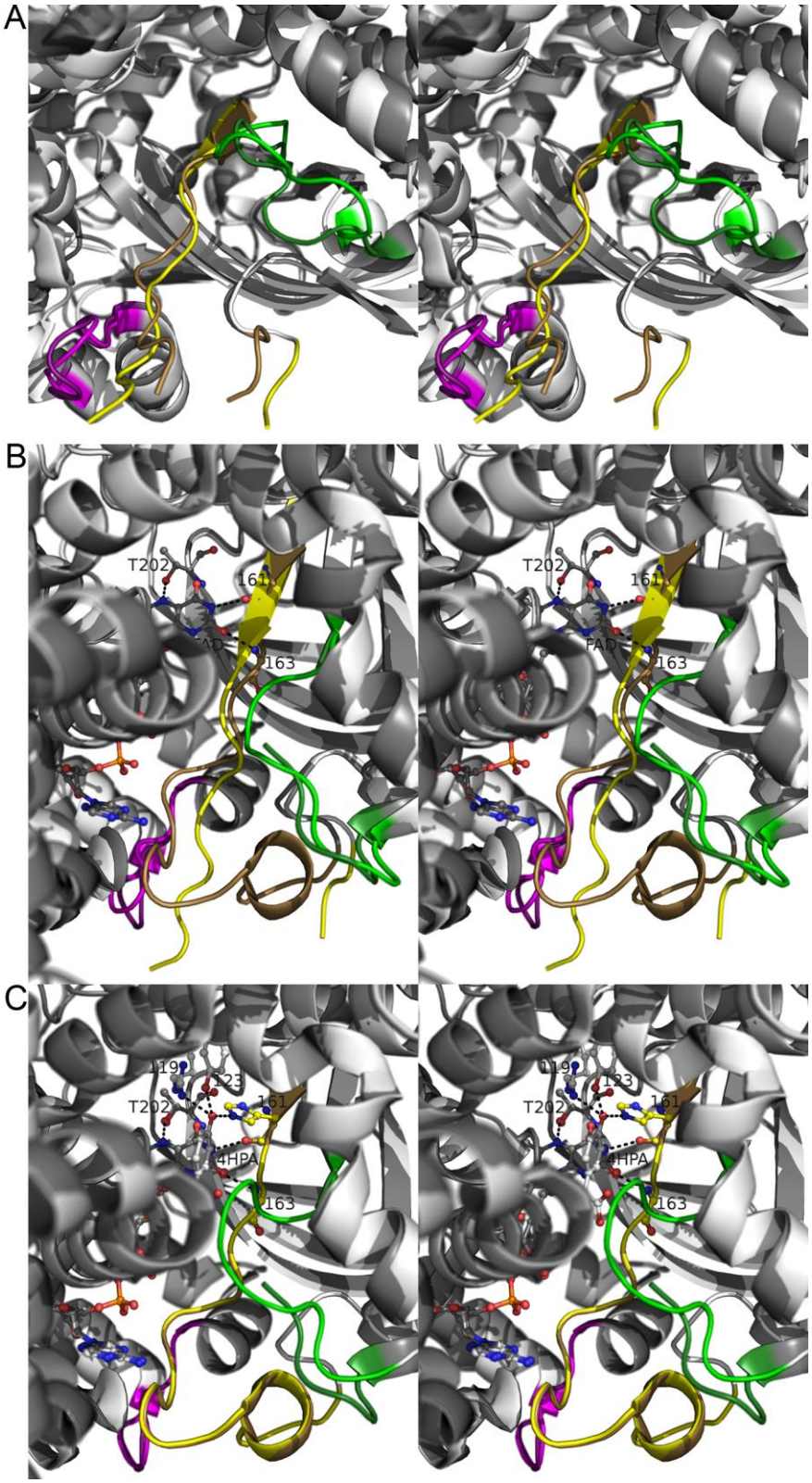

Figure S10. Active site of AbHpaH. The residues are colored similarly to Figure 4C, as the structures of acyl-CoA dehydrogenases and AbHpaH are very similar. The backbone atoms and S171 bind the flavin ring similarly to those of TtHpaB, revealing a conserved flavin binding mode when compared to Figure 5B. The residues bonding to the phenol of 4HPA in TtHpaB/SgcC differ from AbHpaH, nevertheless the C3 carbons of 4HPA in both AbHpaH and TtHpaB are approximately 5 angstroms from the C4a of the flavin. This reveals that resides H120 and S146 of AbHpaH serve similar roles as Y123 and H161 of SgcC/TtHpaB. The residue H396 of AbHpaH likely fulfils the role of R119 of SgcC/TtHpaB, which is likely to form and stabilize the C4a-hydroperoxyflavin intermediate.

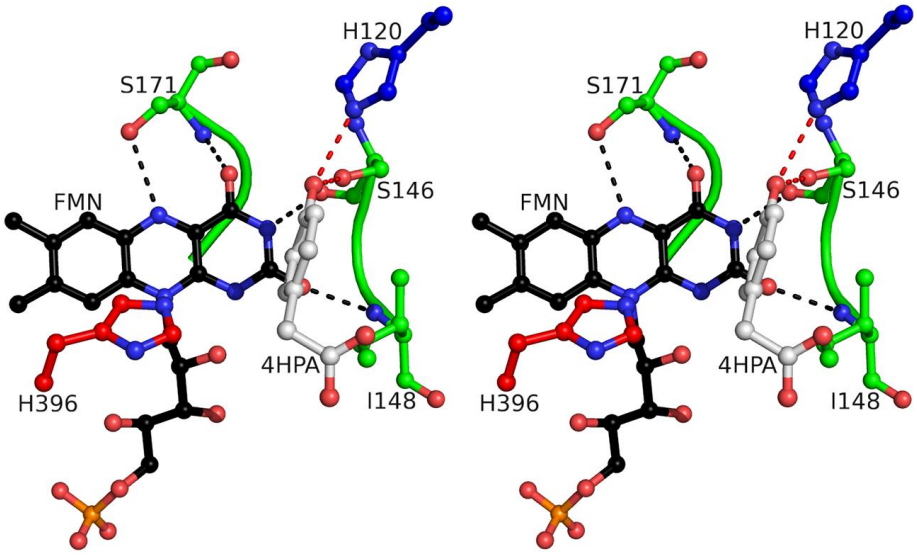

Figure S11. The SgcC-SgcC2 docking model. (a) The functional residues Ser31 (phosphopantetheine-anchored residue, shown in magenta) of SgcC2 points toward the active center of SgcC. (b) SgcC2 is bound at the center of the SgcC tetramer. The four subunits of SgcC are shown in green, cyan, yellow, and blue, respectively, and SgcC2 is shown in gray. The active center of SgcC is shown by *red* dotted circle. (c) The analysis statistics of the interactions between the SgcC tetramer and SgcC2.

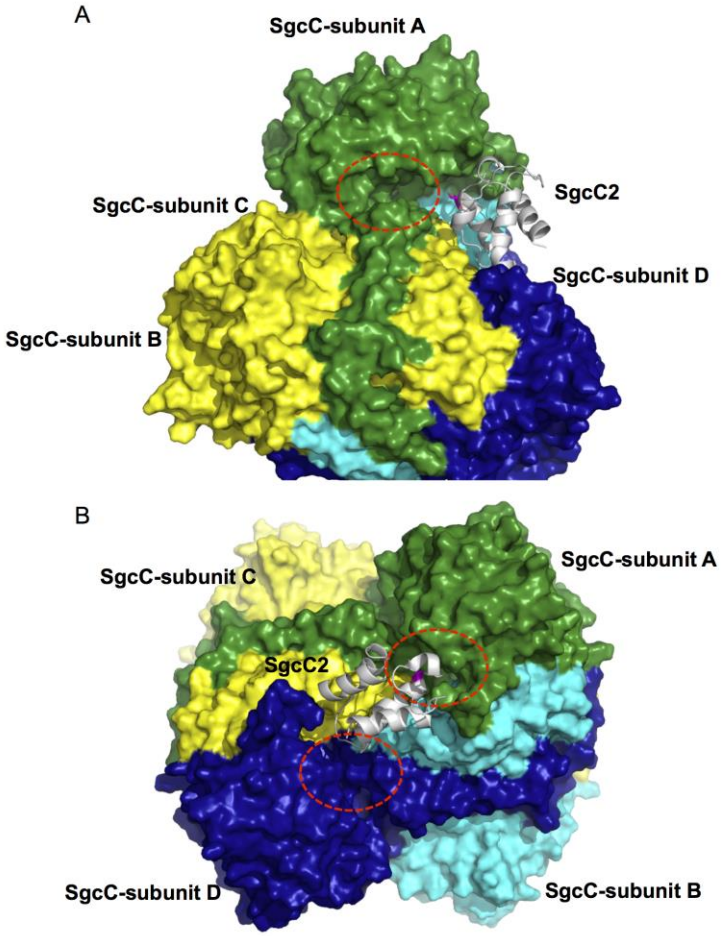

C

Hydrogen bonds

	SgcC-subunit A	Dist. [Å]	SgcC2
1	ARG 170[NH1]	3.70	GLN 30[OE1]
2	ARG 170[NH1]	3.39	GLY 28[O]
3	ARG 170[NH2]	2.87	VAL 13[O]
4	ARG 170[NH2]	3.30	GLY 28[O]
5	LYS 220 [H]	2.48	ILE 25[O]

	SgcC-subunit B	Dist. [Å]	SgcC2
1	ARG 337[NH1]	2.78	GLU 43[OE2]
2	GLY 332 [O]	3.63	ARG 36[NH2]

Salt bridges

	SgcC-subunit B	Dist. [Å]	SgcC2
1	ARG 337[NH1]	2.78	GLU 43[OE2]
2	ASP 335[OD2]	3.61	ARG 36[NE]

References

(1) Van Lanen, S. G., Lin, S., Horsman, G. P., and Shen, B. (2009) Characterization of SgcE6, the flavin reductase component supporting FAD-dependent halogenation and hydroxylation in the biosynthesis of the enediyne antitumor antibiotic C-1027. *FEMS Microbiol. Lett. 300*, 237-241.

(2) Kim, S. H., Hisano, T., Iwasaki, W., Ebihara, A., and Miki, K. (2008) Crystal structure of the flavin reductase component (HpaC) of 4-hydroxyphenylacetate 3-monooxygenase from Thermus thermophilus HB8: Structural basis for the flavin affinity. *Proteins 70*, 718-730.

(3) Kirchner, U., Westphal, A. H., Muller, R., and van Berkel, W. J. (2003) Phenol hydroxylase from Bacillus thermoglucosidasius A7, a two-protein component monooxygenase with a dual role for FAD. *J. Biol. Chem. 278*, 47545-47553.

(4) van den Heuvel, R. H., Westphal, A. H., Heck, A. J., Walsh, M. A., Rovida, S., van Berkel, W. J., and Mattevi, A. (2004) Structural studies on flavin reductase PheA2 reveal binding of NAD in an unusual folded conformation and support novel mechanism of action. *J. Biol. Chem. 279*, 12860-12867.

(5) Webb, B. N., Ballinger, J. W., Kim, E., Belchik, S. M., Lam, K. S., Youn, B., Nissen, M. S., Xun, L., and Kang, C. (2010) Characterization of chlorophenol 4-monooxygenase (TftD) and NADH:FAD oxidoreductase (TftC) of Burkholderia cepacia AC1100. *J. Biol. Chem. 285*, 2014-2027.

(6) Otto, K., Hofstetter, K., Rothlisberger, M., Witholt, B., and Schmid, A. (2004) Biochemical characterization of StyAB from Pseudomonas sp. strain VLB120 as a two-component flavin-diffusible monooxygenase. *J. Bacteriol*. *186*, 5292-5302.

(7) Zhang, Y., Edwards, T. E., Begley, D. W., Abramov, A., Thompkins, K. B., Ferrell, M., Guo, W. J., Phan, I., Olsen, C., Napuli, A., Sankaran, B., Stacy, R., Van Voorhis, W. C., Stewart, L. J., and Myler, P. J. (2011) Structure of nitrilotriacetate monooxygenase component B from Mycobacterium thermoresistibile. *Acta Cryst. F67*, 1100-1105.

(8) Okai, M., Kudo, N., Lee, W. C., Kamo, M., Nagata, K., and Tanokura, M. (2006) Crystal structures of the short-chain flavin reductase HpaC from Sulfolobus tokodaii strain 7 in its three states: NAD(P)(+)(-)free, NAD(+)(-)bound, and NADP(+)(-)bound. *Biochemistry 45*, 5103-5110.

(9) Steinkellner, G., Gruber, C. C., Pavkov-Keller, T., Binter, A., Steiner, K., Winkler, C., Lyskowski, A., Schwamberger, O., Oberer, M., Schwab, H., Faber, K., Macheroux, P., and Gruber, K. (2014) Identification of promiscuous ene-reductase activity by mining structural databases using active site constellations. *Nat. Commun. 5*, 4150.

(10) Christendat, D., Yee, A., Dharamsi, A., Kluger, Y., Savchenko, A., Cort, J. R., Booth, V., Mackereth, C. D., Saridakis, V., Ekiel, I., Kozlov, G., Maxwell, K. L., Wu, N., McIntosh, L. P., Gehring, K., Kennedy, M. A., Davidson, A. R., Pai, E. F., Gerstein, M., Edwards, A. M., and Arrowsmith, C. H. (2000) Structural proteomics of an archaeon. *Nat. Struct. Biol. 7*, 903-909.

(11) Chiu, H. J., Johnson, E., Schroder, I., and Rees, D. C. (2001) Crystal structures of a novel ferric reductase from the hyperthermophilic archaeon Archaeoglobus fulgidus and its complex with NADP+. *Structure 9*, 311-319.

(12) Vadas, A., Monbouquette, H. G., Johnson, E., and Schroder, I. (1999) Identification and characterization of a novel ferric reductase from the hyperthermophilic Archaeon Archaeoglobus fulgidus. *J. Biol. Chem. 274*, 36715-36721.

(13) Galan, B., Diaz, E., Prieto, M. A., and Garcia, J. L. (2000) Functional analysis of the small component of the 4-hydroxyphenylacetate 3-monooxygenase of Escherichia coli

W: a prototype of a new Flavin:NAD(P)H reductase subfamily. *J. Bacteriol. 182*, 627-636.
(14) Lin, S., Van Lanen, S. G., and Shen, B. (2008) Characterization of the two-component, FAD-dependent monooxygenase SgcC that requires carrier protein-tethered substrates for the biosynthesis of the enediyne antitumor antibiotic C-1027. *J. Am. Chem. Soc. 130*, 6616-6623.
(15) Kim, S. H., Hisano, T., Takeda, K., Iwasaki, W., Ebihara, A., and Miki, K. (2007) Crystal structure of the oxygenase component (HpaB) of the 4-hydroxyphenylacetate 3-monooxygenase from Thermus thermophilus HB8. *J. Biol. Chem. 282*, 33107-33117.
(16) Hayes, R. P., Webb, B. N., Subramanian, A. K., Nissen, M., Popchock, A., Xun, L., and Kang, C. (2012) Structural and Catalytic Differences between Two FADH(2)-Dependent Monooxygenases: 2,4,5-TCP 4-Monooxygenase (TftD) from Burkholderia cepacia AC1100 and 2,4,6-TCP 4-Monooxygenase (TcpA) from Cupriavidus necator JMP134. *Int. J. Mol. Sci. 13*, 9769-9784.
(17) Chakraborty, S., Ortiz-Maldonado, M., Entsch, B., and Ballou, D. P. (2010) Studies on the mechanism of p-hydroxyphenylacetate 3-hydroxylase from Pseudomonas aeruginosa: a system composed of a small flavin reductase and a large flavin-dependent oxygenase. *Biochemistry 49*, 372-385.
(18) Furuya, T., and Kino, K. (2014) Catalytic activity of the two-component flavin-dependent monooxygenase from Pseudomonas aeruginosa toward cinnamic acid derivatives. *Appl. Microbiol. Biotechnol. 98*, 1145-1154.
(19) Prieto, M. A., Diaz, E., and Garcia, J. L. (1996) Molecular characterization of the 4-hydroxyphenylacetate catabolic pathway of Escherichia coli W: engineering a mobile aromatic degradative cluster. *J. Bacteriol. 178*, 111-120.
(20) Xun, L., and Sandvik, E. R. (2000) Characterization of 4-hydroxyphenylacetate 3-hydroxylase (HpaB) of Escherichia coli as a reduced flavin adenine dinucleotide-utilizing monooxygenase. *Appl. Environ. Microbiol. 66*, 481-486.
(21) Prieto, M. A., and Garcia, J. L. (1994) Molecular characterization of 4-hydroxyphenylacetate 3-hydroxylase of Escherichia coli. A two-protein component enzyme. *J. Biol. Chem. 269*, 22823-22829.
(22) Duffner, F. M., Kirchner, U., Bauer, M. P., and Muller, R. (2000) Phenol/cresol degradation by the thermophilic Bacillus thermoglucosidasius A7: cloning and sequence analysis of five genes involved in the pathway. *Gene 256*, 215-221.
(23) Stintzi, A., Johnson, Z., Stonehouse, M., Ochsner, U., Meyer, J. M., Vasil, M. L., and Poole, K. (1999) The pvc gene cluster of Pseudomonas aeruginosa: role in synthesis of the pyoverdine chromophore and regulation by PtxR and PvdS. *J. Bacteriol. 181*, 4118-4124.
(24) Clarke-Pearson, M. F., and Brady, S. F. (2008) Paerucumarin, a new metabolite produced by the pvc gene cluster from Pseudomonas aeruginosa. *J. Bacteriol. 190*, 6927-6930.
(25) Liu, X., Dong, Y., Li, X., Ren, Y., Li, Y., Wang, W., Wang, L., and Feng, L. (2010) Characterization of the anthranilate degradation pathway in Geobacillus thermodenitrificans NG80-2. *Microbiology 156*, 589-595.
(26) Hawumba, J. F., Brozel, V. S., and Theron, J. (2007) Cloning and characterization of a 4-hydroxyphenylacetate 3-hydroxylase from the thermophile Geobacillus sp. PA-9. *Curr. Microbiol*. *55*, 480-484.
(27) Kadiyala, V., and Spain, J. C. (1998) A two-component monooxygenase catalyzes both the hydroxylation of p-nitrophenol and the oxidative release of nitrite from 4-nitrocatechol in Bacillus sphaericus JS905. *Appl. Environ. Microbiol. 64*, 2479-2484.

(28) Perry, L. L., and Zylstra, G. J. (2007) Cloning of a gene cluster involved in the catabolism of p-nitrophenol by Arthrobacter sp. strain JS443 and characterization of the p-nitrophenol monooxygenase. *J. Bacteriol. 189*, 7563-7572.
(29) Moncoq, K., Regad, L., Mann, S., Mejean, A., and Ploux, O. (2013) Structure of the prolyl-acyl carrier protein oxidase involved in the biosynthesis of the cyanotoxin anatoxin-a. *Acta Cryst. D69*, 2340-2352.
(30) Watanabe, K., Khosla, C., Stroud, R. M., and Tsai, S. C. (2003) Crystal structure of an Acyl-ACP dehydrogenase from the FK520 polyketide biosynthetic pathway: insights into extender unit biosynthesis. *J. Mol. Biol*. *334*, 435-444.
(31) Alfieri, A., Fersini, F., Ruangchan, N., Prongjit, M., Chaiyen, P., and Mattevi, A. (2007) Structure of the monooxygenase component of a two-component flavoprotein monooxygenase. *Proc. Natl. Acad. Sci. USA 104*, 1177-1182.
(32) Li, Y., Llewellyn, N. M., Giri, R., Huang, F., and Spencer, J. B. (2005) Biosynthesis of the unique amino acid side chain of butirosin: possible protective-group chemistry in an acyl carrier protein-mediated pathway. *Chem. Biol. 12*, 665-675.